MÜHENDİSLİK FAKÜLTESİ

Uluslararası Mühendislik Araştırma ve Geliştirme Dergisi

International Journal of Engineering Research and Development

Cilt/Volume:10 Sayı/Issue:2 Haziran/June 2018 https://doi.org/10.29137/umagd.426804

Araştırma Makalesi / Research Article

Thermal Residual Stresses Analyses of Two-Dimensional Functionally Graded Circular Plates with Temperature-Dependent Material Properties

Munise Didem DEMİRBAŞ [*1], Mustafa Kemal APALAK[1]

[1]Erciyes University, Faculty of Engineering, Mechanical Engineering, 38039, Kayseri
**corresponding author*

Başvuru/Received: 03/02/2018 **Kabul/Accepted**: 27/05/2018 **Son Versiyon/Final Version**: 29/06/2018

Abstract

In this study, thermal residual stress analysis of Functionally Graded Circular Plates joined with adhesive (FGCP-A) is presented. Finite difference equations are used in solving Navier's equations of elasticity and heat transfer. The grading along the plate is made along the surface of the plate. Material properties of the plate are investigated depending on the temperature dependent/independent and it is assumed that the temperature independent material properties changed according to the Mori-Tanaka approach. Grading along the plate is made in both radial and angular directions. In this study, the effects of temperature dependent/independent material properties and compositional gradient exponents on temperature, equivalent strain and equivalent stress are compared. As a result, when considering the properties of the material depending on the temperature, the temperature, equivalent stress and strain distributions and levels vary considerably. Therefore, the properties of the material dependent on the temperature must be taken into consideration in the analysis of thermal residual stress of materials used as high temperature material.

Key Words

Functionally graded circular plates, Finite difference methods, Thermal residual stress, adhesive, temperature-dependent material properties

**mddemirbas@erciyes.edu.tr*

1. INTRODUCTION

The functionally graded materials (FGMs) are one kind of the high technology materials that have been researched to decrease thermal stresses and to eliminate discontinuous stress concentrations (Noda, 1999). FGMs overcome the disadvantage of the conventional composites plates that have been used as thermal barriers in the space planes, ultra-super-hypersonic airplanes for the super-sonic transport, nuclear fusion reactors, and similar structures (Choules and Kokini, 1996).

Moosaie and Panahi-Kalus (2017), presented an analytical solution for nonlinear static thermoelastic analysis of a spherical shell made of two-dimensional functionally graded material. They assumed that the material properties of the plate have changed depending on the temperature. Mehditabar et al. (2017), presented the dynamo-thermo-elastic behavior of a functionally graded hollow cylinder. They used the combined differential quadrature and finite difference methods in their numerical solutions. Ebrahimi and Jafari (2018), investigated the thermo-mechanical behavior of functionally graded beams subjected to thermal loads. They graded the beams functionally in one direction and assumed that the material properties changed depending on the temperature. Manthena and Kedar (2018), investigated the temperature distribution and thermal stress distribution of a functionally graded hollow cylinder with temperature dependent material properties. They solved the two-dimensional transient heat transfer equation under a convective heat transfer condition with a varying point heat source.

In many studies have focused thermo-elastic or plastic stress analyses on the one- or two-dimensional functionally graded plates, and these structures are assumed as a functionally graded composition variation through the thickness (Apalak and bagci, 2011; Apalak, 2014; Nimje and Panigrahi, 2017). Nowadays, fuel cell technology applies successfully FGMs to solid oxide fuel cells in order to reduce thermal expansion coefficient mismatch between electrolyte and anode examined inclusively five categories of fuel cells, and related studies (Iwasawa et al., 1997; Wang et al., 2011). Fuel cells are popular examples that conductive and convective heat transfers, and mass transfer, multiple fluids flows moreover electrochemical reactions are experienced (Kakac, 2007; Ruys et al., 2001; Noda, 1997). Consequently, a tubular or planar design of a solid oxide fuel cell can experience in-plane or through-thickness heat transfer due to heat fluxes. Thus, an in-plane one- or two-dimensional functionally graded materials distribution requires a theoretical investigation for the practical applications.

In this study, thermal residual stress analyses of two-dimensional functionally graded circular plates joined with adhesive are performed for different composite gradient bases and temperature dependent/ independent material properties. For a two-dimensional thermo-elastic problem, Heat Transfer and Navier 's Equations are re-solved using an FDM. The set of linear equations has been solved using the so-called singular value method. The in-plane heat flux is applied from the whole outer edge of the FGCP-A and the inner edge is considered insulated. The effect of temperature-dependent material properties (T-D) and temperature-independent material properties (T-ID) is compared.

2. MATERIALS AND METHODS

In the current study, the Functionally Graded Circular Plates joined with adhesive (FGCP-A) have a material composition of two constituents, ceramic and metal, and the material composition is two-dimensional in the plate plane. The effects of temperature dependent/independent material properties and compositional gradient exponents on temperature, equivalent strain and equivalent stress are investigated. The finite difference method is used in the numerical solution of the thermal stress problem. The finite difference equations of Heat Transfer and Navier's Equations are coded, solved and post-processed graphically in MATLAB mathematical software (Matlab, 2009).

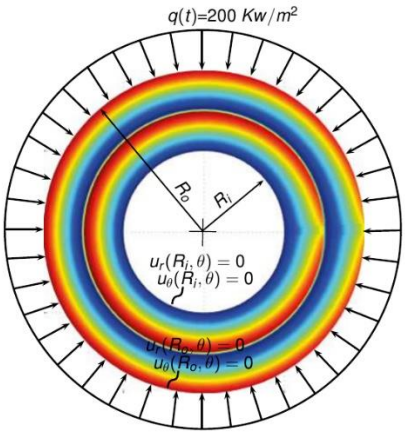

Figure 1. Functionally Graded Circular Plates joined with adhesive (FGCP-A)

2.1. Material Properties

This study is assumed that the FGCP-A are designed as a homogeneous isotropic graded layer along the radial direction between ceramic and metal phases. The material composition of circular plates is Ceramic-Metal-Adhesive-Ceramic-Metal from outside to inside (Figure 1). The volume fraction of the ceramic (c) phase at every all position of the plate follows the power law as (Nemat-Alla, 2003),

$$\mathbf{V_c^r}(\bar{\mathbf{r}}) = \left(\frac{\bar{\mathbf{r}}}{\mathbf{l_R}}\right)^{\mathbf{n}} \tag{1}$$

$$\mathbf{V_c^\theta}(\boldsymbol{\theta}) = (|\mathbf{sin}(\mathbf{p}\boldsymbol{\theta})|)^{\mathbf{m}} \tag{2}$$

n and m compositional gradient exponents along the r- and θ- directions, respectively, $\bar{r}=r-R_i$ is the radial distance from the inner edge of the circular plate, and $l_R=R_o-R_i$ is the FGCP-A length. R_i and R_o are the inner and outer radius of the circular plate, respectively. p=0.5 is a period of periodic functions. The ceramic volume fraction of the plate abides by the power law as

$$\mathbf{V_c}(\bar{\mathbf{r}}, \boldsymbol{\theta}) = \mathbf{V_c^r}(\bar{\mathbf{r}})\mathbf{V_c^\theta}(\boldsymbol{\theta}) \tag{3}$$

for the metal volume fraction of the plate,

$$\mathbf{V_m}(\bar{\mathbf{r}}, \boldsymbol{\theta}) = \mathbf{1} - \mathbf{V_c}(\bar{\mathbf{r}}, \boldsymbol{\theta}) \tag{4}$$

where r and θ are considered as distance along in-plane radial and tangential directions, respectively.

2.2. Temperature-independent material properties

Temperature-independent material properties of the constituents of Ti - 6Al - 4V and ZrO_2 composite material are explained in Table 1. The simple estimation method is the linear rule of the mixtures in which a material properties P at any point r in the graded region are determined.

$$\mathbf{P}(\mathbf{r}) = \mathbf{V_c}(\mathbf{r})\mathbf{P_c}(\mathbf{r}) + \mathbf{V_m}(\mathbf{r})\mathbf{P_m}(\mathbf{r}) \tag{5}$$

Tomota et al. (1976) offered a mixtures rule for the elasticity modulus as Wakashima-Tsukamoto (1991), makes statement necessitate that the overall thermal expansion coefficient (α) for a diphase material is connected the averaged bulk modulus (K) using the Levin relation (1967). The temperature-independent other material properties of the FGCP-A have been accepted to change according to the Mori-Tanaka approach (Mori and Tanaka, 1973).

Table 1. The thermal, physical and mechanical properties of metal (Ti - 6Al - 4V), ceramic (ZrO_2) and adhesive used (Matweb, 2016)

Property	Unit	Ti-6Al-4Vi	ZrO_2	Adhesive
Density, ρ	kg/m^3	4429	5680	1640
Thermal conductivity, λ	W/mK	6.7	1.675	8.121
Specific heat capacity, cp	J/kgK	0.155	0.116	0.16
Coefficient of thermal expansion, α	1/K	8.8^{-6}	2.3^{-6}	40.47^{-6}
Elasticity modulus, E	GPa	113.8	94.5	4.391

2.3. Temperature-dependent material properties

In the literature, the temperature dependence of thermo-mechanical properties of ZrO_2 and Ti - 6Al - 4V are given as follows, respectively (Cubberiy, 1989; Touloukian et al., 1973).

For ZrO_2

$$\lambda = 1.71 + 0.21x10^{-3}T + 0.116x10^{-6}T^2 \quad (W/mK) \tag{6}$$

$$c = 2.74x10^{2} + 7.95x10^{-1}T - 6.19x10^{-4}T^2 + 1.71x10^{-7}T^3 \quad (J/kgK) \tag{7}$$

$$\rho = 3657/\left(1 + \alpha(T - 300)\right)^3 \ (kg/m^3) \tag{8}$$

$$\alpha = 13.31x10^{-6} - 18.9x10^{9}T + 12.7x10^{-12}T^2 \ (1/K) \tag{9}$$

$$E = 1322 - 50.3x10^{-3}T - 8.1x10^{-6}T^2 \ (GPa) \tag{10}$$

$$\nu = 0.333 \tag{11}$$

For Ti - 6Al - 4V

$$\lambda = 1.1 + 0.017T \quad (W/mK) \tag{12}$$

$$c = 3.5x10^{2} + 8.78x10^{-1}T - 9.74x10^{-4}T^2 + 4.43x10^{-7}T^3 \quad (J/kgK) \tag{13}$$

$$\rho = 4420/\left(1 + \alpha(T - 300)\right)^3 \quad (kg/m^3) \tag{14}$$

For $300K \leq T \leq 1100K$ (15)

$$\alpha = 7.43x10^{-6} + 5.56x10^{-9}T - 2.69x10^{-12}T^2 \quad (1/K)$$

For $1100K \leq T$ (16)

$$\alpha = 10.291x10^{-6} \quad (1/K)$$

$$E = 122.7 - 0.00565T \quad (GPa) \tag{17}$$

$$\nu = 0.289 + 32x10^{-6}\,T \tag{18}$$

2.4. Heat Transfer

Transient three-dimensional heat transfer equation where λ is the heat conductivity coefficient, ρ is the density, c_p is the specific heat capacity,

$$\vec{\nabla}\left(\lambda\vec{\nabla}T\right) = \rho c_p \frac{\partial T}{\partial t} \tag{19}$$

$$\frac{\lambda}{r}\frac{\partial T}{\partial r} + \lambda\frac{\partial^2 T}{\partial r^2} + \frac{\lambda}{r^2}\frac{\partial^2 T}{\partial \theta^2} = \rho c_p \frac{\partial T}{\partial t} \tag{20}$$

T (r, θ, t) at the nodal point (i, j) with the coordinate (r,θ) or with respect to time t and the space variables (r,θ). Herewith, the heat transfer equation can be written in terms of difference equations as (for the internal grid points along i= [2: nr-1] and j= [2: nw-1]),

$$T_{i,j}^{k+1} = T_{i,j}^{k} + \frac{\lambda_{i,j}\Delta t}{\left(\rho c_p\right)_{i,j} r_{i,j}\Delta r}\left(T_{i+1,j}^{k} - T_{i,j}^{k}\right) + \frac{\lambda_{i,j}\Delta t}{\left(\rho c_p\right)_{i,j}(\Delta r)^2}\left(T_{i+1,j}^{k} - 2T_{i,j}^{k} + T_{i-1,j}^{k}\right)$$
$$+ \frac{\lambda_{i,j}\Delta t}{\left(\rho c_p\right)_{i,j}\left(r_{i,j}\right)^2(\Delta\theta)^2}\left(T_{i,j+1}^{k} - 2T_{i,j}^{k} + T_{i,j-1}^{k}\right) \tag{21}$$

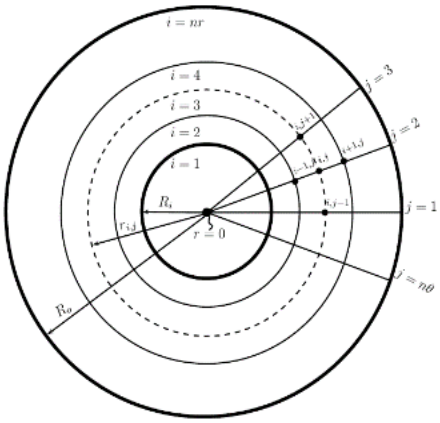

Figure 2. Finite difference grit of FGCP-A

for all grid points at i=1 and j= [1: nw],

$$T_{i,j}^{k+1} = T_{i,j}^{k} + \frac{\lambda_{i,j}\Delta t}{(\rho c_p)_{i,j} r_{i,j}\Delta r}\left(T_{i+1,j}^{k} - T_{i,j}^{k}\right) + \frac{\lambda_{i,j}\Delta t}{(\rho c_p)_{i,j}(\Delta r)^2}\left(-T_{i+3,j}^{k} + 4T_{i+2,j}^{k} - 5T_{i+1,j}^{k} + 2T_{i,j}^{k}\right) + \frac{\lambda_{i,j}\Delta t}{(\rho c_p)_{i,j}(r_{i,j})^2(\Delta\theta)^2}\left(T_{i,j+1}^{k} - 2T_{i,j}^{k} + T_{i,j-1}^{k}\right) \quad (22)$$

for all grid points at i=nr and j= [1: nw],

$$T_{i,j}^{k+1} = T_{i,j}^{k} + \frac{\lambda_{i,j}\Delta t}{(\rho c_p)_{i,j} r_{i,j}\Delta r}\left(T_{i,j}^{k} - T_{i-1,j}^{k}\right) + \frac{\lambda_{i,j}\Delta t}{(\rho c_p)_{i,j}(\Delta r)^2}\left(-T_{i-3,j}^{k} + 4T_{i-2,j}^{k} - 5T_{i-1,j}^{k} + 2T_{i,j}^{k}\right) + + \frac{\lambda_{i,j}\Delta t}{(\rho c_p)_{i,j}(r_{i,j})^2(\Delta\theta)^2}\left(T_{i,j+1}^{k} - 2T_{i,j}^{k} + T_{i,j-1}^{k}\right) \quad (23)$$

this equations can be arranged on thermal equilibrium of that cell as follows: for all grid points at

i= [2: nr-1], j=1 to $j - 1 \rightarrow nw$ (24)

i= [2: nr-1], j=nw to $j + 1 \rightarrow 1$ (25)

are written.

2.4.1. Initial and Boundary Conditions

The initial temperature is given as $T(r,\theta)$=298 K at t=0, and thermal boundary conditions are given as:

$$q_i = q(R_i, \theta, t) \quad (26)$$

$$q_o = q(R_o, \theta, t) = 200\text{KW/m}^2 \quad (27)$$

Where $q_i = q_f$ and $q_o = q_e$ are inner and outer heat fluxes along the radial direction r, respectively. The boundary condition, the inner edge is subjected to adiabatic conditions while the outer boundary is subjected to heat flux. The initial temperature is taken as 298 K for the whole FGCP-A and the analysis is completed when the temperature reached 393 K at any point along the adhesive. The inner and outer radius of FGCP-A is 100 mm and 200 mm, respectively. The radial length of each plate is 48 mm and the radial length of the adhesive is 4 mm. FGCP-A has a total radial length l=100 mm and thickness t=1mm. As the 1 mm plate thickness is much smaller than other dimensions, the stress and strain in the thickness direction are neglected and a 2-D analyses is conducted.

If the first boundary condition is adapted to the two-dimensional heat transfer equation, (along the outer edge of the FGCP-A ($r_{nr,j}$= R_o) with (i=1, j= [1: nw]))

$$\frac{(\rho c_p)_{i,j}}{\lambda_{i,j}\Delta t}\left(T_{i,j}^{k+1} - T_{i,j}^{k}\right) = \frac{2q_e}{\lambda_{i,j}\Delta r} + \frac{2}{(\Delta r)^2}\left(T_{i-1,j}^{k} - T_{i,j}^{k}\right) + \frac{1}{(\Delta\theta)^2}\left(T_{i,j+1}^{k} - T_{i,j}^{k}\right) + \frac{1}{(\Delta\theta)^2}\left(T_{i,j-1}^{k} - T_{i,j}^{k}\right) \quad (28)$$

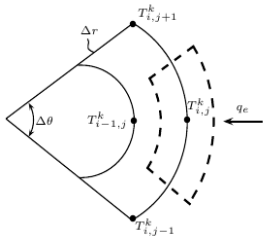

Figure 3. Outer edge of plate

If the second boundary condition is adapted to the two-dimensional heat transfer equation, (along the inner edge of the FGCP-A ($r_{nr,j}$= R_i) with (i=1, j= [1: nw]))

$$\frac{(\rho c_p)_{i,j}}{\lambda_{i,j}\Delta t}\left(T_{i,j}^{k+1}-T_{i,j}^{k}\right)=\frac{2q_f}{\lambda_{i,j}\Delta r}+\frac{2}{(\Delta r)^2}\left(T_{i+1,j}^{k}-T_{i,j}^{k}\right)+\frac{1}{(\Delta\theta)^2}\left(T_{i,j+1}^{k}-T_{i,j}^{k}\right)+\frac{1}{(\Delta\theta)^2}\left(T_{i,j-1}^{k}-T_{i,j}^{k}\right) \tag{29}$$

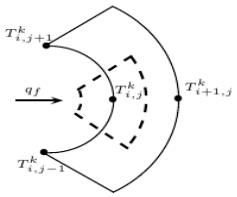

Figure 4. Inner edge of plate

2.5. Navier's Equations of Elasticity

Two-dimensional Navier's equations of elasticity in the radial and tangential directions are written as ($T=T(r,\theta,t)-T_o$ is the temperature difference)

$$\left(r\frac{\partial u}{\partial r}-u+r^2\frac{\partial^2 u}{\partial r^2}\right)-\left(\frac{\lambda+3\mu}{\lambda+2\mu}\right)\frac{\partial v}{\partial\theta}+\left(\frac{\lambda+\mu}{\lambda+2\mu}\right)r\frac{\partial^2 v}{\partial r\partial\theta}+\left(\frac{\mu}{\lambda+2\mu}\right)\frac{\partial^2 u}{\partial\theta^2}-\left(\frac{3\lambda+2\mu}{\lambda+2\mu}\right)r^2\alpha\frac{\partial T}{\partial r}=0 \tag{30}$$

$$\frac{\partial^2 v}{\partial\theta^2}+\left(\frac{\lambda+3\mu}{\lambda+2\mu}\right)\frac{\partial u}{\partial\theta}+\left(\frac{\lambda+\mu}{\lambda+2\mu}\right)r\frac{\partial^2 u}{\partial r\partial\theta}+\left(\frac{\mu}{\lambda+2\mu}\right)\left(r\frac{\partial v}{\partial r}-v+r^2\frac{\partial^2 v}{\partial r^2}\right)-\left(\frac{3\lambda+2\mu}{\lambda+2\mu}\right)r\alpha\frac{\partial T}{\partial\theta}=0 \tag{31}$$

In equations (30) and (31), the thermal stress equations are written for the entire plate by choosing the appropriate ones from the equations (32)-(43) for the finite difference equations with the first and second order derivatives (in the inner region and edges of the plate).

$$\frac{\partial\varpi}{\partial r}=\frac{\varpi_{i+1,j}-\varpi_{i,j}}{\Delta r} \tag{32}$$

$$\frac{\partial\varpi}{\partial r}=\frac{\varpi_{i,j}-\varpi_{i-1,j}}{\Delta r} \tag{33}$$

$$\frac{\partial\varpi}{\partial\theta}=\frac{\varpi_{i,j+1}-\varpi_{i,j}}{\Delta\theta} \tag{34}$$

$$\frac{\partial\varpi}{\partial\theta}=\frac{\varpi_{i,j}-\varpi_{i,j-1}}{\Delta\theta} \tag{35}$$

$$\frac{\partial^2\varpi}{\partial r^2}=\frac{\varpi_{i+1,j}-2\varpi_{i,j}+\varpi_{i-1,j}}{(\Delta r)^2} \tag{36}$$

$$\frac{\partial^2\varpi}{\partial\theta^2}=\frac{\varpi_{i,j+1}-2\varpi_{i,j}+\varpi_{i,j-1}}{(\Delta\theta)^2} \tag{37}$$

$$\frac{\partial^2\varpi}{\partial r^2}=\frac{-\varpi_{i+3,j}+4\varpi_{i+2,j}-5\varpi_{i+1,j}+2\varpi_{i,j}}{(\Delta r)^2} \tag{38}$$

$$\frac{\partial^2 \varpi}{\partial \theta^2} = \frac{-\varpi_{i,j+3} + 4\varpi_{i,j+2} - 5\varpi_{i,j+1} + 2\varpi_{i,j}}{(\Delta\theta)^2} \tag{39}$$

$$\frac{\partial^2 \varpi}{\partial r^2} = \frac{-\varpi_{i-3,j} + 4\varpi_{i-2,j} - 5\varpi_{i-1,j} + 2\varpi_{i,j}}{(\Delta r)^2} \tag{40}$$

$$\frac{\partial^2 \varpi}{\partial \theta^2} = \frac{-\varpi_{i,j-3} + 4\varpi_{i,j-2} - 5\varpi_{i,j-1} + 2\varpi_{i,j}}{(\Delta\theta)^2} \tag{41}$$

$$\frac{\partial^2 \varpi}{\partial r\, \partial \theta} = \frac{\varpi_{i,j+1} - \varpi_{i,j} - \varpi_{i-1,j+1} + \varpi_{i-1,j}}{\Delta r \Delta\theta} \tag{42}$$

$$\frac{\partial^2 \varpi}{\partial r\, \partial \theta} = \frac{\varpi_{i,j} - \varpi_{i,j-1} - \varpi_{i-1,j} + \varpi_{i-1,j-1}}{\Delta r \Delta\theta} \tag{43}$$

2.5.1. Initial and boundary conditions

The FGCP-A is fixed along all its edges (u (r, θ) =0 and v (r, θ) =0). The material is completely ceramic (ZrO_2) at r =148 mm and r=200 mm, and the material is completely metal (Ti-6Al-4V) at r =100 mm and r=152 mm in FGCP-A. A one-dimensional grading is performed along radial direction with three different compositional gradient exponents of n = 0.1 (ceramic rich compound), 1.0 (linear change is from ceramic rich compound to metal rich compound) and 10.0 (metal rich compound). In order to determine the influence of the properties of the material depending on the temperature, the composition gradient exponents in the radial direction is kept constant on the inner and outer plates. Therefore, the composition gradient exponents in the radial direction is indicated only by 'n' for both plates. The compositional gradient exponent in the tangential direction is kept constant at m=1.0 (linear change is from ceramic rich compound to metal rich compound).

FDM requires that the FGCP-A be divided into a grid of nr = 80 x nq = 240 divisions along the coordinates r and θ, respectively. The division number is 38 and 4 for plates and adhesive, respectively. The temperature matrix obtained from the heat transfer solution is considered as the temperature difference in the Navier equations. The appropriate finite difference equations are selected for the internal points, edges and corners of the plate. The implicit difference equations of the stress analysis are coded, solved and post-processed graphically in MATLAB (Matlab, 2009).

3. RESULTS

In this study, the effect of temperature-dependent material properties and the compositional gradient exponents on the thermo-elastic behavior of the FGCP-A with adhesively bonded is investigated using the FDM. The material properties of the adhesive for all analyses are temperature independent.

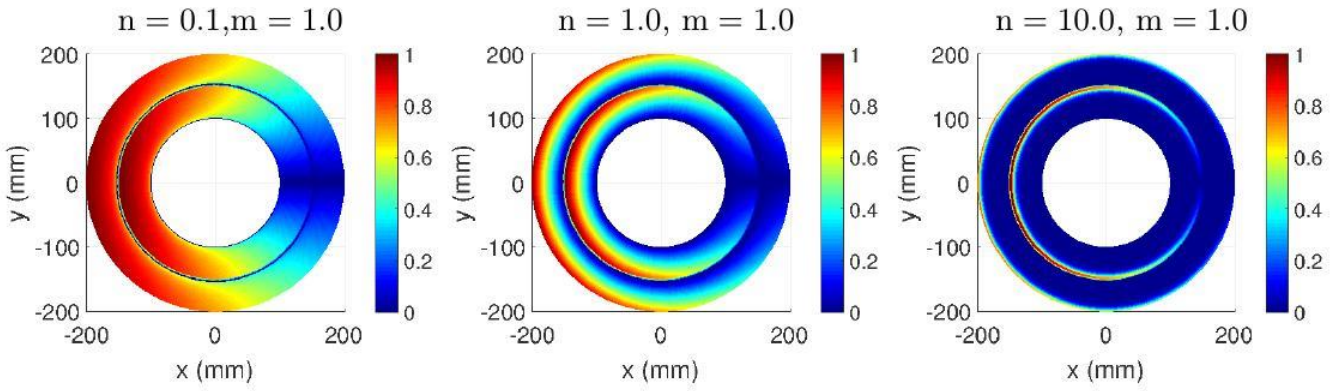

Figure 5. Distribution of the compositional gradient exponents along the FGCP-A for different compositional gradients

As shown in Figure 5, the composition in the tangential direction for all FGCP-A is m = 1. For this reason, there is a linear variation in the tangential direction. If the FGCP-A is divided into two pieces in the vertical axis, the plate regions on the right side are rich in metal and the plate regions on the left are rich in ceramics. As the composition gradient increases from the top value n = 0.1 to 10, the ceramic composition decreases in the composition of the regions on the left side of the plates (Figure 5).

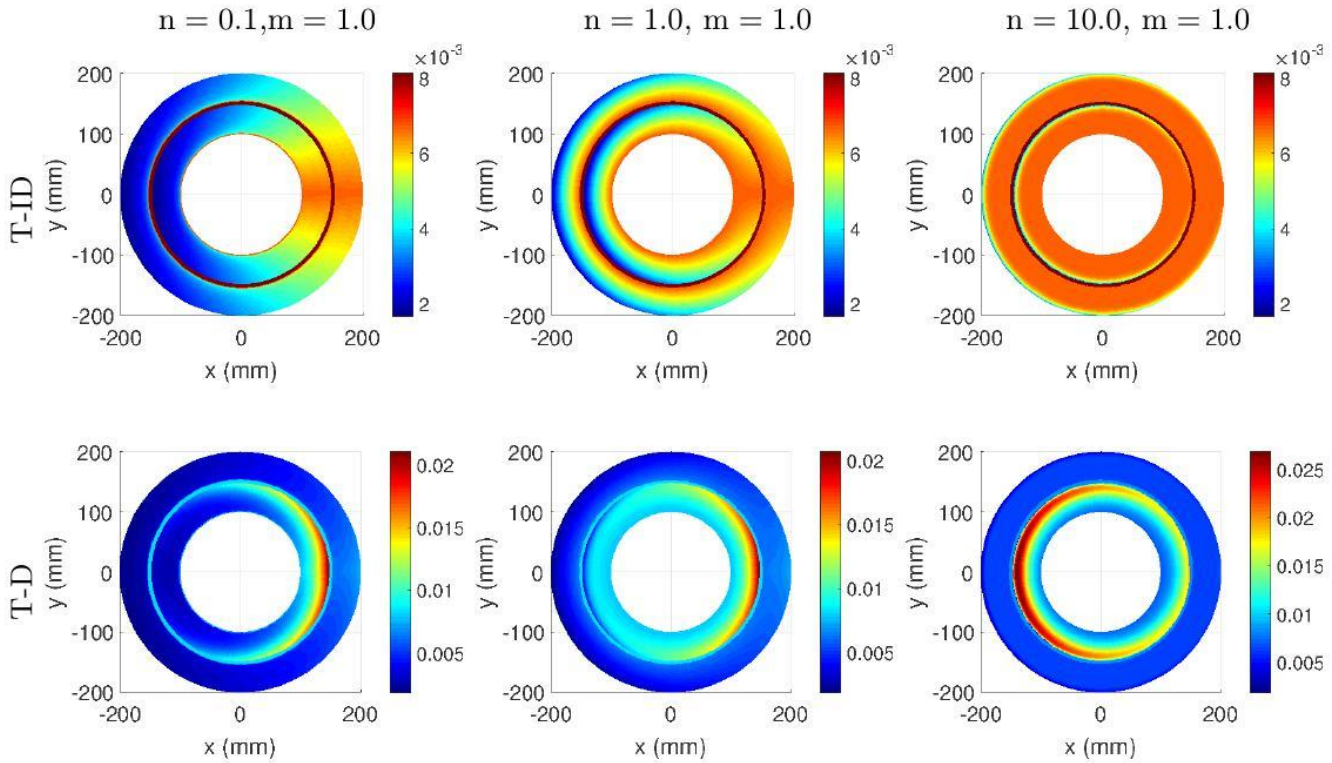

Figure 6. Distribution of the in-plane coefficient of thermal conductivity along the FGCP-A for different compositional gradients in both T-ID/T-D cases

Figure 6 shows the distribution of the coefficient of thermal conductivity along the plates for temperature dependent and independent material properties. The coefficient of thermal conductivity of the metal and ceramic is significantly increased for T-D cases.

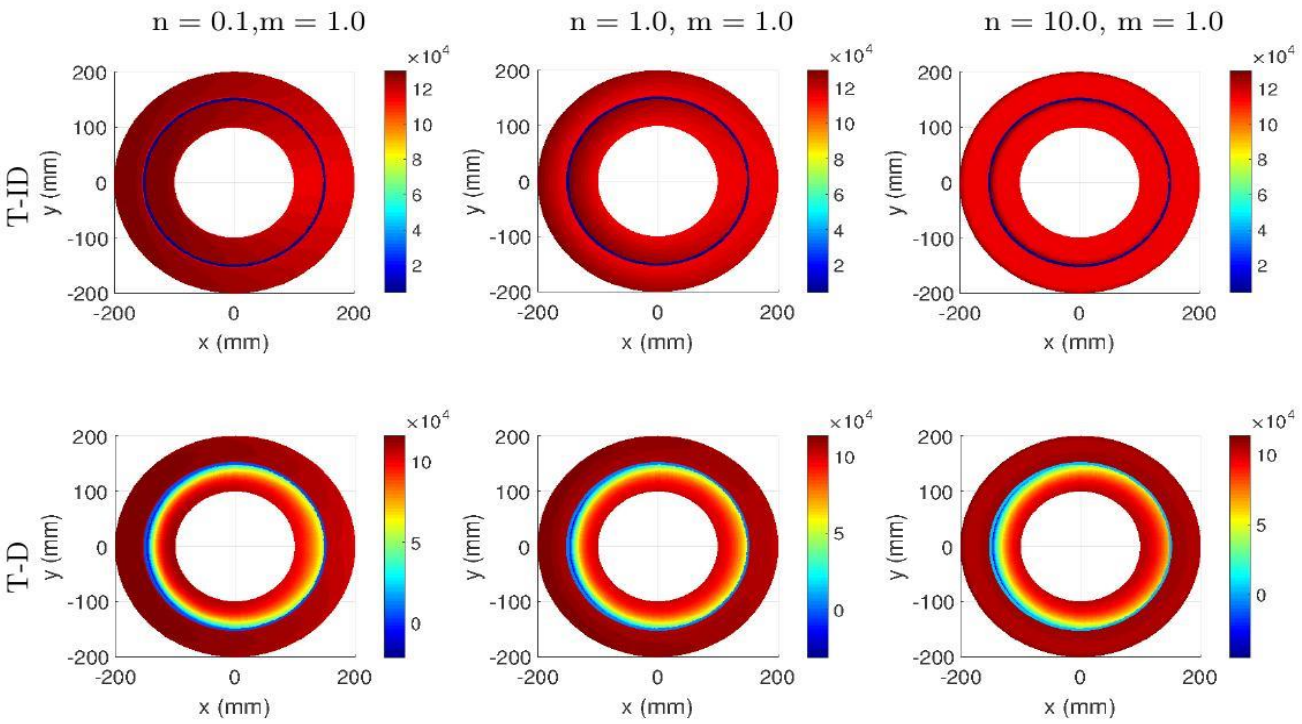

Figure 7. Distribution of the in-plane the elasticity modulus along the FGCP-A for different compositional gradients in both T-ID/T-D cases

Figure 7 shows the distribution of the modulus of elasticity along the plates for temperature dependent and independent material properties at different composition gradient exponents. Modulus of elasticity is reduced in temperature effect of ceramic and metal materials. This decrease in levels is higher in ceramics than in metals.

All material properties such as Poisson's ratio, density, coefficient of thermal expansion, specific thermal capacity coefficient vary in temperature effect. However, in this work, as a thermal material property, the thermal conductivity coefficient and the elasticity modulus as a mechanical material property are shown in the figures. For other material properties, levels will be mentioned. The density of the ceramic material decreases depending on the temperature. Metal material does not change significantly. The specific heat capacity of ceramic and metal materials increases with the temperature. This increase is greater in ceramic materials. If the material properties change depending on the temperature, the coefficient of thermal expansion of the ceramic and metal increases. This increase is greater in ceramic materials. While the Poisson ratio in ceramics increases with temperature, the metal materials do not change significantly.

Table 2: Effects of material properties of T-D/T-ID and compositional gradient exponents on the critical temperatures, equivalent strains and equivalent stress in the FGCPs-A.

		T(K)	ε_{eqv}	σ_{eqv}(MPa)
n=0.1	T-ID	2047	0.01137	2282
	T-D	2243	0.031	5744
n=1.0	T-ID	2306	0.0125	2289
	T-D	2356	0.031	5744
n=10.0	T-ID	2540	0.026	2380
	T-D	2506	0.056	6089

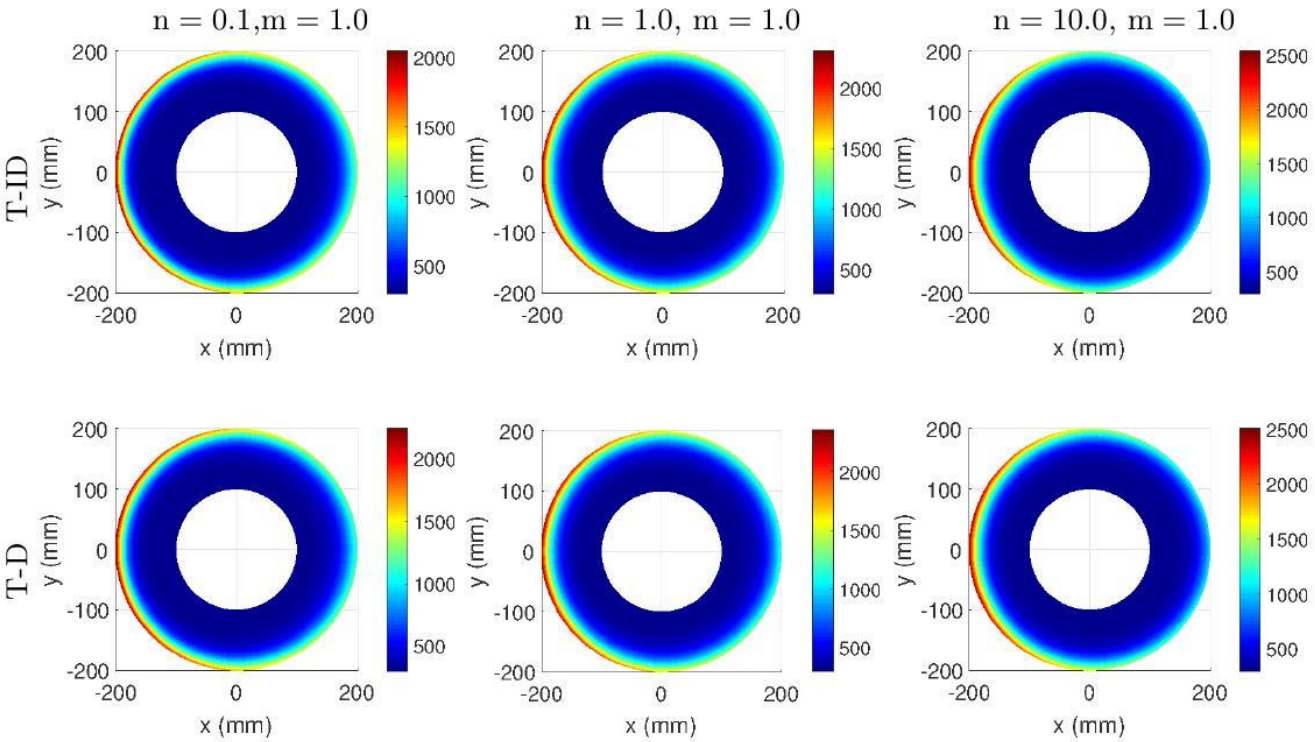

Figure 8. Distribution of the in-plane temperature along the FGCP-A for different compositional gradients in both T-ID/T-D cases.

Figure 8 shows the temperature distributions along the plate for T-D and T-ID cases at different compositional gradient exponents in the radial direction. The temperature distribution throughout the connection does not change significantly. However, in the case of T-D for n = 0.1 and 1, the difference between the maximum temperature levels with respect to the T-ID case increases by 196 and 49 K, respectively. For n=10, in T-D case, the difference according to T-ID case is decreased by 34K (Table 2). At n=10 the compound is rich in metal. The metal material is less affected by temperature than the ceramic material.

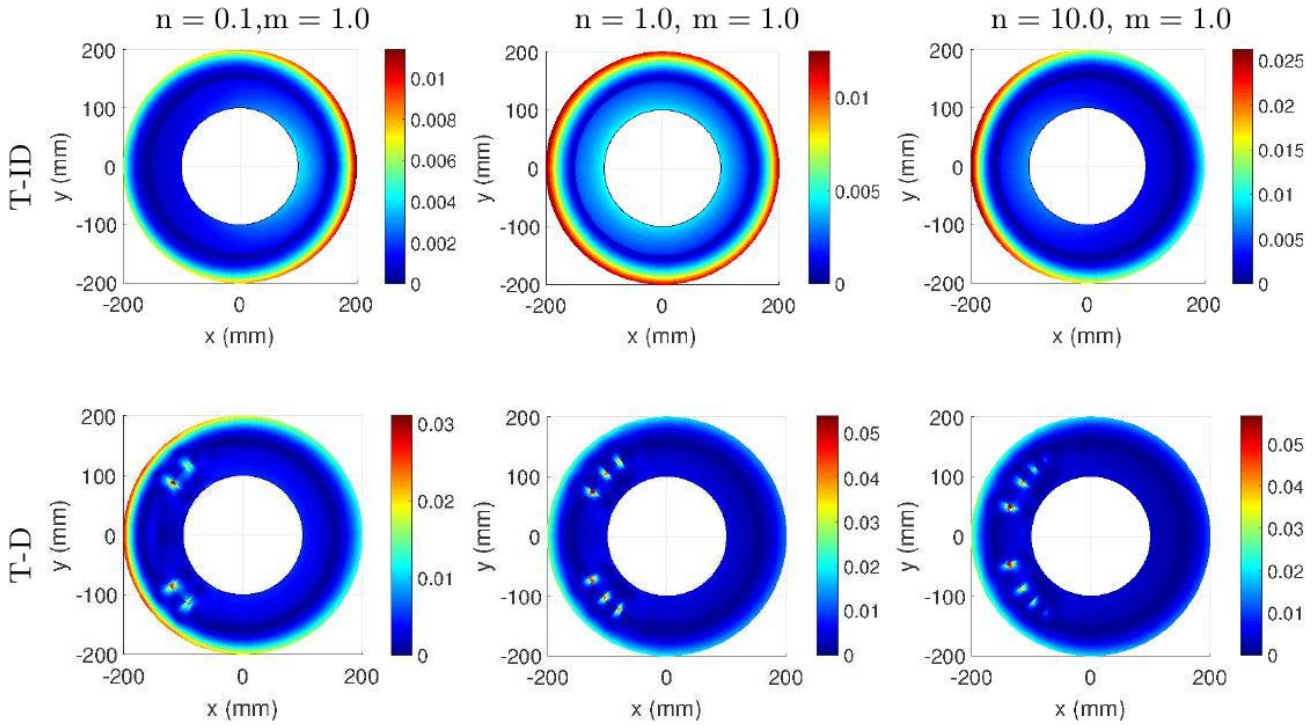

Figure 9. Distribution of the in-plane equivalent strain along the FGCP-A for different compositional gradients in both T-ID/T-D cases.

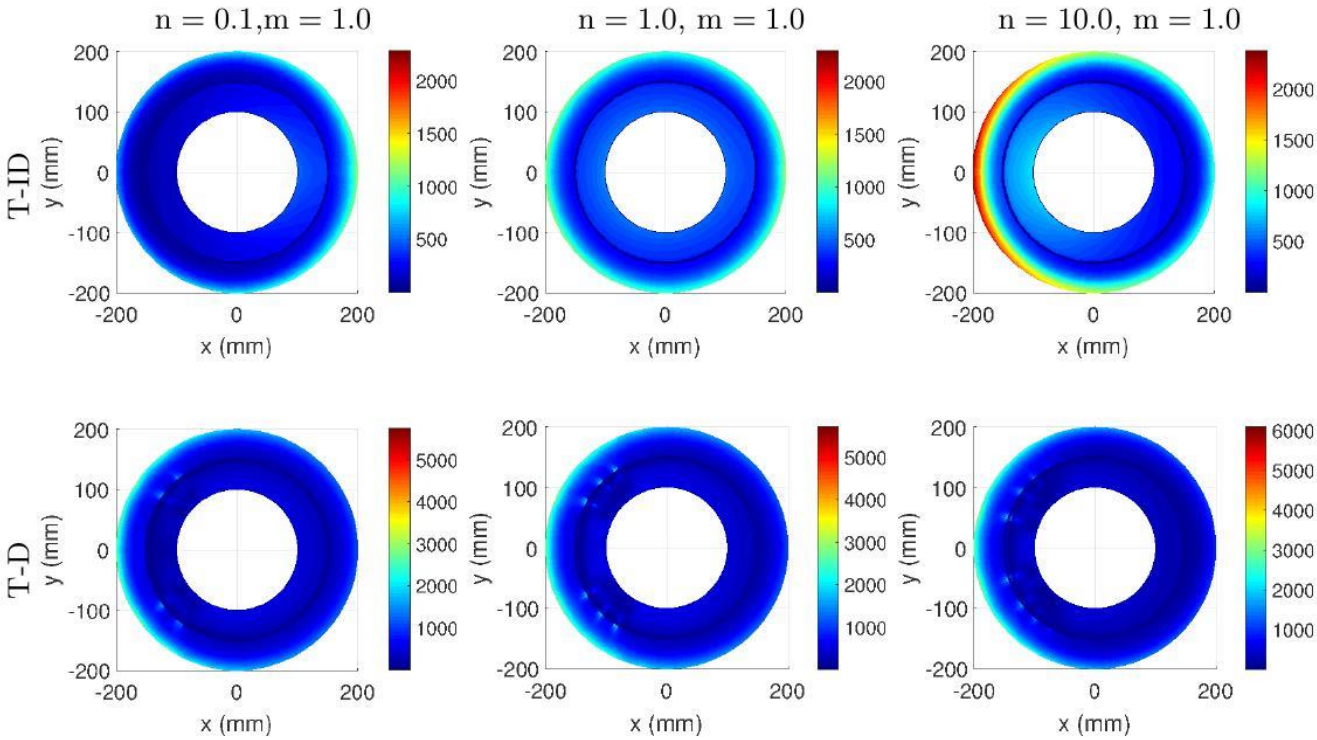

Figure 10. Distribution of the in-plane equivalent strress along the FGCP-A for different compositional gradients in both T-ID/T-D cases.

Figure 9 shows the distribution of equivalent strain along the connection in T-D/T-ID material properties for different compositional gradient exponents. In the case of T-D, the difference between the maximum equivalent strain levels with respect to the T-ID case is 0.019, 0.0185 and 0.03 for n = 0.1, 1.0 and 10.0, respectively.

When m=1.0 is constant, the equivalent stress distribution varies with the composition in the radial direction (n). For T-ID cases, the maximum strain region at n=0.1 is observed along the outer edge on the right side of the FGCP-A. In T-D cases, this region is observed along the outer edge on the left side of the FGCP-A. For T-ID cases, the maximum strain region at n=1.0 is observed along the outer edge of the FGCP-A. In T-D cases, these region is observed along the outer edge on the left side of the FGCP-A.

In the case of T-ID and T-D, the maximum strain regions at m = 10.0 are observed along the outer edge on the left side of the FGCPs. In the case of T-D, the equivalent strain levels vary locally due to thermal and mechanical changes in the adhesive and outer plate interface (Figure 9).

Figure 10 shows the distribution of equivalent stress along the FGCP-A material properties for different compositional gradient exponents in T-D/T-ID cases. In the case of T-D, the difference between the maximum equivalent strain levels with respect to the T-ID case is 3461, 3455 and 3709 MPa for n = 0.1, 1.0 and 10.0, respectively. At n=0.1 the maximum stress regions are seen as semicircular along the outer edge on the left and right sides of FGCP-A, respectively, for T-ID and T-D cases.

The maximum stress regions at n=1.0 are seen in a circular along the outer edge of the FGCP-A in the case of T-ID, and semi-circularly along the outer edge in the left side of the FGCP-A in the case of T-D. For n = 10, in both T-D and T-ID cases, the maximum stress regions are observed semi-circularly along the outer edge of the left side of the plate. In all compositions, in the case of T-D, also on the left side of the plate there are medium levels of stress regions in the adhesive and outer plate interface.

3.1. Conclusions

In this study, the effects of temperature dependent / independent material properties and compositional gradient exponents on temperature, equivalent strain and equivalent stress levels and their distribution in the FGCP-A are investigated.

As shown in the study, when considering the properties of the material depending on the temperature, the temperature, equivalent stress and strain distributions and levels vary considerably. In addition, when material properties are taken into account, depending on the temperature, significant stress zones occur at the adhesive interface. In this study emphasizes the necessity of taking into consideration the temperature-dependent material properties in the thermal stress analysis of functionally graded circular plates bonded with adhesive.

For this reason, the properties of the material dependent on the temperature must be taken into consideration in the analysis of the thermal residual stresses of the materials used as the high temperature material.

REFERENCES

Noda, N. (1999). Thermal stress intensity factor for functionally gradient plate with an edge crack. Journal of Thermal Stresses. 22(4-5), 477-512. doi: 10.1080/01495739708956108.

Choules, B.D. & Kokini, K. (1996). Architecture of functionally graded ceramic coatings against surface thermal fracture. Journal of Engineering Materials and Technology. 118(4). 522-528. doi: 10.1115/1.2805951.

Moosaie, A. & Panahi-Kalus, H. (2017). Thermal stresses in an incompressible FGM spherical shell with temperature-dependent material properties. Thin-Walled Structures. 120. 215-224. doi: 0.1016/j.tws.2017.09.005.

Mehditabar, A., Rahimi, G.H. & Tarahhomi, M.H. (2017). Thermo-elastic analysis of a functionally graded piezoelectric rotating hollow cylindrical shell subjected to dynamic loads. Mechanics of Advanced Materials and Structures. 1. 1-12. doi:10.1080/15376494.2017.1329466.

Ebrahimi, F. & Jafari, A. (2018). A four-variable refined shear-deformation beam theory for thermo-mechanical vibration analysis of temperature-dependent FGM beams with porosities. Mechanics of Advanced Materials and Structures. 25(3). 212-224. doi:10.1080/15376494.2016.1255820.

Manthena, V.R. & Kedar, G.D. (2018). Transient thermal stress analysis of a functionally graded thick hollow cylinder with temperature-dependent material properties. Journal of Thermal Stresses. 41(5). 568-582. doi: 10.1080/01495739.2017.1402669.

Apalak, M.K. & Bagci, M.D. (2011). Thermal residual stresses in adhesively bonded in-plane functionally graded clamped circular hollow plates. Journal of Adhesion Science and Technology. 25. 1861-1908. doi:10.1080/01694243.2012.747732.

Apalak, M.K. (2014). Functionally graded adhesively bonded joints. Reviews of Adhesion and Adhesives. 1. 56-84. doi: 10.1002/9781119162346.ch3.

Nimje, S.V. & Panigrahi, S.K. (2017). Stress and failure analyses of functionally graded adhesively bonded joints of laminated frp composite plates and tubes: a critical review. Reviews of Adhesion and Adhesives. 5(2). 162-194. doi: 10.1002/9781119526445.ch5.

Iwasawa C., Nagata, M., Seino, Y. & Ono, M. (1997). A study on anode materials and structures for SOFC. Proceedings of the Fifth International Symposium on Solid Oxide Fuel Cells (SOFC-V). 97(40). 626-634.

Wang, Y., Chen, K.S., Mishler, J., Cho, S.C. & Adroher, X.C. (2011). A review of polymer electrolyte membrane fuel cells: Technology, applications, and needs on fundamental research. Applied Energy. 88(4). 981-1007. doi: 10.1016/j.apenergy.2010.09.030.

Kakac, S., Pramuanjaroenkij, A. & Zhou, X.Y. (2007). A review of numerical modeling of solid oxide fuel cells. International Journal of Hydrogen Energy. 32(7). 761-786. doi: 10.1016/j.ijhydene.2006.11.028.

Ruys, A., Popov, E., Sun, D., Russell, C. & Murray, C. (2001). Functionally graded electrical/thermal ceramic systems. Journal of the European Ceramic Society. 21(10-11). 2025-2029. doi:10.1016/S0955-2219(01)00165-0.

Noda, N. (1997). Thermal stresses intensity factor for functionally gradient plate with an edge crack. J. Therm. Stresses. 20. 373-387. doi: 10.1080/01495739708956108.

Nemat-Alla, M. (2003). Reduction of thermal stresses by developing two-dimensional functionally graded materials. International Journal of Solids and Structures. 40(26). 7339-7356. doi:10.1007/s00707-008-0136-1.

Tomota, Y., Kuroki, K., Mori, T. & Tamura T. (1976). Tensile deformation of two-ductile-phase alloys: flow curves of $\alpha \rightarrow \gamma$ Fe–Cr–Ni alloys. Mater. Sci. Eng. 24. 85-94. doi:10.1016/0025-5416(76)90097-5.

Wakashima, K. & Tsukamoto, H. (1991). Mean-field micromechanics model and its application to the analysis of thermomechanical behavior of composite materials. Mater. Sci. Eng. A. 146. 291-316. doi:10.1016/0921-5093(91)90284-T.

Levin, V.M. (1967). On the coefficients of thermal expansion of heterogeneous material. Mech. Solids. 2. 88-94.

Mori, T. & Tanaka, K. (1973). Average stress in matrix and average elastic energy of materials with misfittings inclusions. Acta Metallurgica. 21(5). 517-574.

Materials Information Resource MatWeb [Online]. (2016). Available: http://www.matweb.com.

Cubberiy, W.H. (1989). Properties and selection: nonferrous alloys and pure metals. Metal Handbook Ninth Edition. ASM. Metals Park. Ohio. vol.2.

Touloukian, Y.S., Powell, R.W., Ho, C.Y. & Nicolaou, M.C. (1973). thermophysical properties of matter-the tprc data series, volume 10. thermal diffusivity. IFI Plenum. New-York. Washington. vol.10.

Matlab. (2009). Mathematical software. version 2009a. TheMathWorks.